6. Supplemental Material

In the following section, some additional information is provided, which did not fit into the paper due to the limited space.

6.1. Rotation Matrix

In the end of Subsection 3.1 the well-known rotation matrix $\mathbf{R}$ is used:

$$\begin{aligned}\mathbf{R} &= \mathbf{R}_z(\alpha)\mathbf{R}_y(\beta)\mathbf{R}_x(\gamma)\\ &= \begin{pmatrix} \cos\alpha*\cos\beta & \cos\alpha*\sin\beta*\sin\gamma-\sin\alpha*\cos\gamma & \cos\alpha*\sin\beta*\cos\gamma+\sin\alpha*\sin\gamma \\ \sin\alpha*\cos\beta & \sin\alpha*\sin\beta*\sin\gamma+\cos\alpha*\cos\gamma & \sin\alpha*\sin\beta\cos*\gamma-\cos\alpha*\sin\gamma \\ -\sin\beta & \cos\beta*\sin\gamma & \cos\beta*\sin\gamma \end{pmatrix}.\end{aligned} \tag{6}$$

6.2. Example

The stiffness tensor

$$\mathbf{C}_\mathrm{K} = \begin{pmatrix} 0.555124 & -0.680203 & -0.850148 & 0.355314 & 0.171874 & -0.323865 \\ -0.680203 & 1.16136 & -2.34536 & -0.329882 & -0.637087 & -0.13137 \\ -0.850148 & -2.34536 & 1.21676 & 0.00356122 & 0.0164092 & 1.07961 \\ 0.355314 & -0.329882 & 0.00356122 & 0.803498 & 0.320542 & 0.00710463 \\ 0.171874 & -0.637087 & 0.0164092 & 0.320542 & 1.47928 & 0.284946 \\ -0.323865 & -0.13137 & 1.07961 & 0.00710463 & 0.284946 & 1.48702 \end{pmatrix} \tag{7}$$

can be rotated into its natural coordinate system. Therefore, the multipoles (see Equation 4) and the resulting symmetry plane normals must be calculated. Following this, the normals for this tensor are $\mathbf{n}_1 = \begin{pmatrix}-0.909653 & -0.349183 & 0.224951\end{pmatrix}^T$, $\mathbf{n}_2 = \begin{pmatrix}-0.401904 & 0.603137 & -0.688984\end{pmatrix}^T$, and $\mathbf{n}_3 = \begin{pmatrix}0.104905 & -0.717145 & -0.688984\end{pmatrix}^T$. The tensor is, according to these normals, orthotropic and the angles for the rotation can be calculated by the Euler angles of the rotation of the normal system onto the coordinate axes. There are multiple possibilities to rotate the normals onto the coordinate axes. One example is given by the angles $\gamma = -57.2095$, $\beta = 65.4574$, and $\alpha = -14.6289$. Thus, the rotated tensor is

$$\mathbf{C}_\mathrm{K}^R = \begin{pmatrix} -0.484848 & -1.09091 & -0.606061 & 0 & 0 & 0 \\ -1.09091 & -0.454545 & -0.363636 & 0 & 0 & 0 \\ -0.606061 & -0.363636 & 0.242424 & 0 & 0 & 0 \\ 0 & 0 & 0 & 1.4 & 0 & 0 \\ 0 & 0 & 0 & 0 & 2 & 0 \\ 0 & 0 & 0 & 0 & 0 & 4 \end{pmatrix}. \tag{8}$$

Comparing this tensor with the general orthotropic stiffness tensor

$$\mathbf{c}^\mathrm{K}_\mathrm{ortho} = \begin{pmatrix} \frac{1-\nu_{23}\nu_{32}}{D}E_1 & \frac{\nu_{13}\nu_{32}+\nu_{12}}{D}E_2 & \frac{\nu_{12}\nu_{23}+\nu_{13}}{D}E_3 & 0 & 0 & 0 \\ \frac{\nu_{13}\nu_{32}-\nu_{12}}{D}E_2 & \frac{1-\nu_{13}\nu_{31}}{D}E_2 & \frac{\nu_{21}\nu_{13}+\nu_{23}}{D}E_3 & 0 & 0 & 0 \\ \frac{\nu_{12}\nu_{23}+\nu_{13}}{D}E_3 & \frac{\nu_{21}\nu_{13}+\nu_{23}}{D}E_3 & \frac{1-\nu_{12}\nu_{21}}{D}E_3 & 0 & 0 & 0 \\ 0 & 0 & 0 & 2G_{23} & 0 & 0 \\ 0 & 0 & 0 & 0 & 2G_{13} & 0 \\ 0 & 0 & 0 & 0 & 0 & 2G_{12} \end{pmatrix}, \tag{9}$$

where

$$D = 1-\nu_{12}\nu_{21}-\nu_{13}\nu_{31}-\nu_{23}\nu_{32}-2\nu_{12}\nu_{23}\nu_{31} \tag{10}$$

the inverse of it, described in Equation 2, can be used to calculate the moduli.

6.3. Ogden material model

Analyses of biological materials often use formulations from the family of Ogden models [Ogd72] or other hyperelastic models given by the strain energy density ψ, i.e., the elastic energy per unit volume. In the sequel, the following variant of the Ogden model, implemented into the open-source finite element software FEBio [EAW12], is used

$$\psi = \frac{1}{2}c_p(J-1)^2 + \frac{c_1}{m_1^2}\left(\lambda_1^{m_1}+\lambda_2^{m_1}+\lambda_3^{m_1}-3-m_1\ln J\right), \tag{11}$$

where λ_i are the principal stretches,

$$J = \det\mathbf{F} = \lambda_1\lambda_2\lambda_3, \tag{12}$$

and c_1, c_p and m_1 are material parameters. $\mathbf{F}$ is the deformation gradient, a second-order two-point tensor. The stiffness tensor in the reference configuration can be described by the derivation of the strain energy density with respect to the right-Cauchy-green tensor $\mathbf{C}$ by

$$\mathcal{C} = 4\frac{\partial^2\psi}{\partial\mathbf{C}^2}. \tag{13}$$

In this work, spatial stiffness tensor data from the current configuration are analyzed without taking into account the finite kinematics required to deform the material to its current state. Instead, the data are simply interpreted in terms of material properties commonly used for linear elastic orthotropic materials as small perturbations on an unknown state.

6.4. Videos

We provide three videos showing fiber surfaces and attribute spaces:

1. *nineDimensionalOverview.mp4*,
2. *twelveDimensionalHighE.mp4*,
3. *BoundaryConditionsOverview.mp4*.

The first time step is excluded in the videos because it shows the basic state, where the sphere is not pushed into the block. This means that the whole material of the block behaves in an isotropic manor and all extracted invariants should be zero. Because of the vast amount of calculations needed to compute the invariants and extract the fiber surfaces, fiber surfaces are extracted in the first step due to rounding errors.

The first video shows the distribution of the nine-dimensional attribute space built of the Young's moduli E_i [1_x_1], the shear moduli G_{ij} [2_x_2], and the Poisson ratios ν_{ij} [4_x_4]. The overview is split into four super parts (separated through the black lines [1_x_1, 2_x_2, 4_x_4]), showing fiber surfaces in the physical domain (a Euclidean space, where the considered block exists), except the lower left part [3_x_3], which shows the used hyper planes to extract the fiber surfaces. Each super part can be split into four subparts [y_1, ..., y_4], where the lower-left subpart [y_3] shows the considered three-dimensional subspace of the nine-dimensional coefficient space and the distribution of the values defined on the grid of the block inside this space using multiple views. The other subparts show fiber surfaces from different viewing angles [y_1, y_2, y_4], constructed using one hyper plane each and restricting only one dimension. The fiber surfaces are color-coded to identify which hyper plane (shown in the lower-left super part [3_x_3]) corresponds to which fiber surface. As example, the red fiber surface in the upper left subpart of the upper left super part [1_1] corresponds to the red hyper plane in the upper left subpart of the lower-left super part

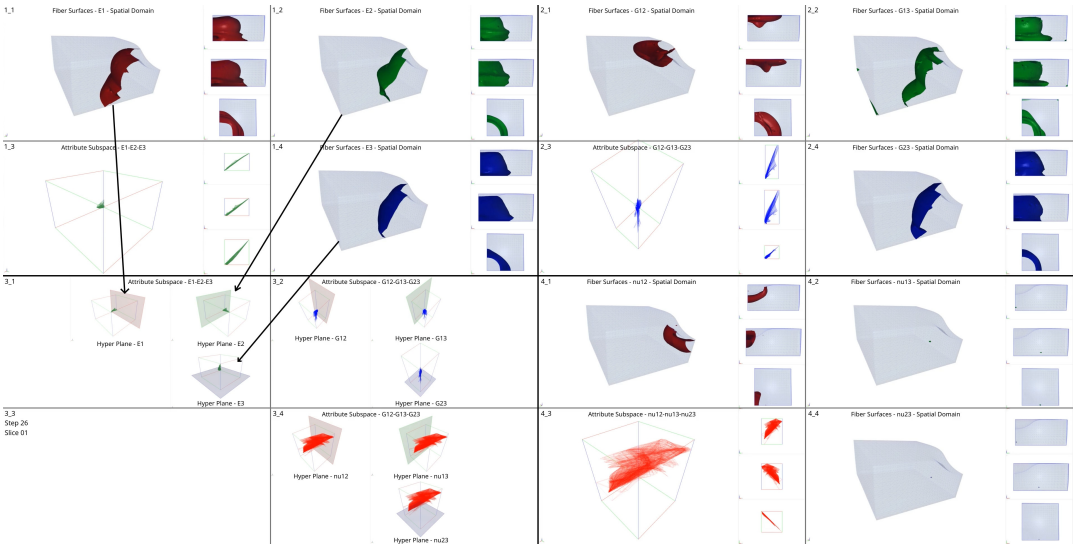

Figure 4: *Example for the relation of the fiber surfaces and their hyper planes used to construct them.*

[3_1] (see Figure 4). Each analyzed time step consists of ten slices, where each of the nine hyper planes is moved into another place for each slice. In general, they are moved from the minimal value of their corresponding dimension to its maximum, excluding both ends.

The second video is also split into five super parts [1_x_1, ..., 5_x_5], where each super part shows the distribution of the remaining values inside each subspace. As described in Subsection 4.3, the considered domain and attribute space is filtered due to high Young's moduli [3_x_3, 4_x_4]. This is visualized in the lower-left super parts [3_x_3, 4_x_4], which show the subspace of Young's moduli and a blue hyper plane sliding along the diagonal from the minimum to the maximum of the bounding box of all values [3_x_3]. In the meantime, when this hyper plane moves to the maximum, the corresponding fiber surfaces are shown rigth next to them [4_x_4]. Furthermore, the hyper plane increasingly restricts the region of interest resulting in smaller extracted regions the closer the hyper plane gets to the maximum. The extracted region is then visualized inside three of the remaining subspaces: shear moduli (top left super part [1_x_1]), Poisson ratios (top right super part [2_x_2]), and right Cauchy-Green tensor eigenvalues (bottom right super part [5_x_5]). To compare the distribution of the values of the extracted region to the values of the whole block, the values of the restricted region are shown in dark colors and the ones of the whole block in lighter colors.

The third video is split into four super parts [1_x_1, ..., 4_x_4] and four subparts [y_1, ..., y_4], each in the same way as the first video, with the only difference, that the lower-left super part [3_x_3] now also shows a three-dimensional subspace. Also, the ordering of the subspaces changed a little bit as a 12-dimensional space is used as the base, which was constructed by adding the eigenvalues of the right Cauchy-Green tensor GEV_i to the nine-dimensional coefficient space [4_x_4]. Additionally, not the whole domain is used. It is reduced in the first step, where the lower part of the block is extracted using the fiber surface extraction algorithm because it was fixed at the bottom in the simulation. Each of the 12 dimensions in this extracted region was sliced in the same way as in the first video using one hyper plane per dimension.